Novel Tm^{3+}-doped fluorotellurite glasses with enhanced quantum efficiency

H. Gebavi [1,*], D. Milanese[1], R. Balda[2], M.Ivanda[3], F. Auzel[4], J. Lousteau[1], J. Fernandez[2], M. Ferraris[1]

[1]Dipartimento di Scienza dei Materiali ed Ingegneria Chimica, Politecnico di Torino, Corso Duca degli Abruzzi 24, 10129 Torino, Italy, email: gebavi@yahoo.com

[2]Departamento de Fisica Aplicada I, Escuela Superior de Ingenieros, Alda. Urquijo s/n 48013 Bilbao, Spain and Center of Materials Physics CSIC-UPV/EHU and Donostia International Physics Center, Apartado 1072, 20080 San Sebastian, Spain

[3]Rudjer Boskovic Institute, Bijenicka c. 54, P.O. Box 180, 10002 Zagreb, Croatia

[4]FAC, Le Mesnils Saint Denis, France

Abstract

In this paper, new highly Tm^{3+}-doped tellurite glasses with host composition $75TeO_2 – xZnF_2 – yGeO_2 – 12PbO – 3Nb_2O_5$ [x(5–15), y(0–5)mol%] are presented and compared to the Tm-doped tellurite glasses based on the traditional host composition: $75TeO_2 – 20ZnO – 5Na_2O$ mol%. Enhanced quantum efficiency from $^3F_4$ level was observed for the proposed glasses and thermal stability and viscosity values make them suitable for optical fiber drawing. Besides the host composition, substantial influence of Tm^{3+} concentration on luminescence and lifetime of excited $^3F_4$ and $^3H_4$ states were discussed.

Keywords: fluorotellurite glass, thulium, Judd-Ofelt, energy transfer.

1. Introduction

Silica based glasses are widely used for optical fiber fabrication for telecommunications and high power fiber lasers, but different glass hosts are employed for more specific applications such as remote sensing, medical surgery and gas monitoring because they offer higher rare earth solubility and lower phonon energies required to allow the fabrication of short cavity lasers operating in the eye-safe, near infrared wavelength region ranging from 1.5 to 2 μm [1, 2, 3].

The choice of a glass able to host high amounts of rare – earth (RE) ions plays an important role in targeting specific optical properties and performances. In the seventies, tellurite glasses were proposed for their high laser cross sections [4] and their weak self-quenching at high active ion concentration [5]. In 1994 Wang [6] proposed tellurite glasses, in

particular the TeO_2 – ZnO – Na_2O (TZN) glass system and concluded that such composition was a good candidate for fiber drawing. The main characteristics of tellurite glasses are wide transmission region (0.35-5μm), good thermal stability, low phonon energy, and high linear and nonlinear refractive index.

In this study two different host compositions were used: a) $75TeO_2$ – $20ZnO$ – $5Na_2O$ (TZN) as first proposed by Wang [6] and a second one which belongs to the group of fluorotellurite glasses b) $75TeO_2$ – $xZnF_2$ – $yGeO_2$ – $12PbO$ – $3Nb_2O_5$ (FTG). Some recent works have been carried out on the compositions similar to the last one. In particular the composition $75TeO_2$ – $10ZnO$ – $10PbO$ – $5Nb_2O_5$ doped with a small concentration of Tm^{3+} targeting 1.47 μm emission for amplifier application was developed [7]. One year later, the composition $75TeO_2$ – $10ZnO$ – $4.5PbO$ – $0.5PbF_2$ – $9.4Nb_2O_5$ doped with $0.6Tm_2O_3$ was patented and a thermal stability factor of 104°C (the difference between crystallization and glass transition temperature) achieved, but no luminescence characteristics report was attached [8]. V. Nazabal [9] in 2003 reported $66TeO_2$ – $10GeO_2$ – $9ZnO$ – $16ZnF_2$ host composition with the Er^{3+} as dopant. The most recent publication is from G. Liao [10] in 2009 where compositions of passive glasses were $(85 – x)TeO_2$ – $xZnF_2$ – $12PbO$ – $3Nb_2O_5$ (x = 0 – 40 mol%).

In FTG composition presented in this study tellurium oxide is a dominant component and plays the role of glass former. Chemical compounds such as zinc fluoride and germanium oxide are added in order to tune specific properties such as minimization of OH content and improvement of thermal stability, respectively.

GeO_2 plays the role of a glass former and its substitution of ZnF_2 aims at increasing refractive index and improving mechanical properties as well. Similar approach was reported for silica glasses [11].

ZnF_2 plays a similar role as ZnO due to similar ionic radius: depolymerization of the glass amorphous structure by increasing TeO_3 units. The increasing amount of ZnF_2 has a stronger effect than ZnO, but weaker than Na_2O. Each zinc ion is surrounded by six fluorine ions and each fluorine is surrounded by three zinc ions. The substitution of ZnO by ZnF_2 in the TZN host composition linearly decreases refractive index [12].

Niobium (V) oxide increases linear and nonlinear refractive index, thermal stability, stability towards crystallization, and chemical durability [13, 14]. No influence on phonon energy has been observed.

Lead (II) oxide (PbO) decreases glass stability: binary TeO_2 – PbO ($T_x - T_g < 50°$ C) glass composition is less stable than TeO_2 – Na_2O ($T_x - T_g \sim 120°$ C). It enters the glass structure as intermediate, creating Pb – O – Pb linkages and because of that changing trigonal bipyramid (tbp) and trigonal pyramid (tp) ratio [12]. In a binary composition PbO plays the role of a network modifier [15]. Decrease of T_g with increasing PbO content is also observed in germanate glasses where it was explained as a consequence of tetrahedral to octahedral coordination change of Ge atoms [16]. Thanks to its higher polarizability compared to ZnO in the TZN host, it leads to increase of refractive index [12].

This study was focused on the multi-component fluorotellurite glass family (named with the acronym "FTG") which was compared to the already well known: TeO_2:ZnO:Na_2O glass (acronym "TZN"). The main idea was to develop novel rare earth doped tellurite glass compositions with improved emission properties in the IR region with respect to state of the art tellurite glasses. For such a purpose thulium was used as an active ion with concentration up to 10.4 10^{20} cm^{-3} targeting emission at around 1.8 μm through transition from $^3F_4$ excited level to $^3H_6$ ground state. Basic glass characterization was performed in order to collect the necessary data for preparation of the fiber drawing process. All these parameters are presented

in the following sections. The influence of host composition and Tm^{3+} concentration on the IR emission from levels $^3F_4$ and $^3H_4$ are also discussed.

The novel proposed host should be considered as the promising photonic material with possible applications for short cavity fiber lasers, infrared amplifiers and different light emitting diodes [17, 18].

2. Experimental techniques

2.1. Glass fabrication

Glasses were prepared by melt quenching from mix powder batches, inside a glove box in a dry atmosphere with water content of about 7 ppm. The chemicals employed (together with their purity) were the following: TeO_2 (99+%), ZnO (99.99%), Na_2CO_3 (99.995%), ZnF_2 (99%), PbO (99.99%), GeO_2 (99.99%), Nb_2O_5 (99.9%), Tm_2O_3 (99.99%). Relative molar ratio of the host glass constituent oxides was kept the same for all samples, regardless of Tm^{3+} doping. The fabricated samples were based on the two host glass compositions $75TeO_2 – 20ZnO – 5Na_2O$ and $75TeO_2 – xZnF_2 – yGeO_2 – 12PbO – 3Nb_2O_5$ [x(5–15), y(0–5)mol%] doped with increasing amounts of Tm^{3+} (1, 3, 5 mol%). Glass melting was carried out in Pt crucible at around 900 °C for 4h, then pouring on a preheated brass plate at 300 °C and annealing followed. The whole process required around 30 h of operation.

2.2 Glass characterization: thermo – mechanical properties

Thermal analysis was performed on fabricated glasses using a Perkin Elmer DSC-7 differential scanning calorimeter up to 550°C under Ar flow with a heat rate of 10°C/min in Al pans using 30 mg glass samples. Thermal analysis was employed to determine the effect of

glass composition on glass stability which can be measured with the quantity T_x-T_g (T_x is crystallization peak onset values and T_g is glass transition temperature).

Viscosity measurements are obtained by parallel–plate method (ASTM C1350M) on Perkin Elmer TMA 7 Thermal Analysis System. Samples were cylindrical shaped with height of 4-6 mm and 4.5 mm in diameter. Applied static force was 100 mN with temperature gradient of 5 °C/min.

Viscosity measurements play a crucial role in determining the temperature at which the fiber drawing process occurs. It is assumed that the drawing process takes place at a temperature corresponding to a viscosity value of 10^4 Pa s ($\log(\eta) \sim 4$). Standard viscosity points which can be found in literature [19, 20] are used to extrapolate the experimental data by fitting using the Vogel - Fulcher - Tammann - Hesse (VFTH) theoretical curve as the boundary conditions.

Experimental data were processed using Gent's equation [21]:

$$\eta = \frac{2 \cdot \pi \cdot F \cdot h^5}{3 \cdot V \cdot (\frac{dh}{dt}) \cdot (2 \cdot \pi \cdot h^3 + V)} \quad (1)$$

where: F – applied force, g = 9.81m/s^2, h – sample height, V – sample volume.

VFTH equation is used to describe non – Arrhenius behavior of glasses. It can be applied on wide temperature range with 10% accuracy [22]:

$$\log(\eta) = \mathrm{A} + \frac{B}{T - T_0} \quad (2)$$

where: $\mathrm{A} = \log(\eta_0)$, $B = \frac{D \cdot T_0}{\ln 10}$, D is strength parameter, and T_0 is diverging temperature.

There are two characteristic points at which different kind of glasses should have similar viscosity value. First of them is the viscosity value at T_g and the other one is at high temperature, where $T_g/T \rightarrow 0$. In both cases, since different glass compositions should have similar structure complexity, the viscosity converges to the same value. Value of viscosity at T_g is widely accepted as $\sim 10^{12}$ Pa s [23]. At high temperature glass complexity of any glass composition decreases and many experimental values indicate the value of A = -5 [24, 25] which defines second characteristic point.

Two kind of fits were made, for the fix parameter A = -5 and A = -4. Difference in calculated drawing temperature for fixed point 'A' in these two cases is ~1°C and because of that, precise value of parameter 'A' does not play a crucial role for drawing process. Because of all these reasons and to simplify the fitting, a fixed value of A = - 5 will be used.

2.3 *Glass characterization: structural properties*

Structural features of the glasses with changing Tm^{3+} concentration were recorded by means of Raman spectroscopy. The instrument used was Jobin Yvon T64000, triple monochromator working in subtractive mode with Coherent Innova 100 argon ion laser at wavelength 514.5 nm used for the excitation.

Specific glass structural order in the low frequency region, creates an excess of the vibrational density of states $g(\omega)_{exc.} = g(\omega) - g(\omega)_{Debye}$, in comparison with Debye model which results in broad band, so called 'boson – peak' (BP) parameterized as '$g(\omega)/\omega^2$' [24]. Martin and Brenig model for reduced Raman intensity in the low frequency region is given by equation $I_R(\omega,T) = C(\omega)g(\omega)/\omega^2$ where $C(\omega)$ is a constant representing average coupling between incident light and the vibration modes of frequency 'ω' called Raman coupling coefficient; and $g(\omega)$ is the density of vibrational state (DVS) [27]. Debye model can not interpret $g(\omega)$, and $C(\omega)$ has no maximum as well so the interpretation of the BP stays a

subject of debate. There are numerous models which propose its origin: dipolar interaction between some defects [28], involment of soft anharmonic potentials [29], fraction - like dynamics of fractal structure [30], combination of acoustic phonons and rotational molecular modes [31].

Boson peak (BP) is temperature dependent and its position varies from 20 to 150 cm^{-1} depending on the host's composition. For example, in silica glass its reduced intensity ($I^{red}(\omega) \propto g(\omega)C(\omega)/\omega^2$ where $g(\omega)$ is the vibrational density of states, $C(\omega)$ is the Raman coupling coefficient) decreases as temperature rises while the row data shows opposite behavior. The true excess $g(\omega)_{exc.}$ decreases in frequency and band area as temperature increases. BP position in the same case increases with temperature up to glass transformation point, remains constant up to the melting point, and then decreases [32]. Annealing process can induce some changes on the BP located in its low energy side involving blue frequency shift and decrease in intensity. Quenching rate will also influence BP amplitude making it more intense [33].

Doping with small concentration of RE ions will cause an increase in BP intensity, but BP intensity decreases when devitrification process starts to occur. Addition of RE is correlated with changes in the concentrations of non-bridging anions. Typical value of such critical concentration when RE solubility limit is reached is about 2000 ppm of Pr^{3+} in $Ge_{34}5S_{55}5I_{10}$ and 10 000 ppm in $70(Ga_2S_3)30(La_2S_3)$ glass [34]. Similar BP amplitude quenching is observed in $70TeO_2 – 30ZnO$ glass for 1 mol% doping with Er_2O_3 [35].

The low-frequency Raman scattering of light is due to the vibrational modes that are localized by the disorder [36]. Vibrational spectrum of homogeneous elastic spherical particles was first proposed by Lamb [37] and further developed by Duval who showed that only spheroidal modes with spherical harmonic function of degree $l = 0$ (spheroidal) and $l = 2$ (ellipsoid) are Raman active [38]. This approach has been further developed for determination

of size distribution of free (weak interacting) nanoparticles [39] and the nanoparticles embedded in matrix [40].

The frequency of the lowest spherical – energy mode of free particle is given by [38]:

$$\omega_s = \frac{0.7 \cdot v_l}{D \cdot c} \tag{3}$$

where D is the sphere diameter, c is light speed and v_l is longitudinal acoustic speed.

For torsional mode a similar equation is proposed: $\omega_s = \frac{0.85 \cdot v_s}{D \cdot c}$ where v_s is shear acoustic velocity. In the literature parameter 'D' is interpreted as a correlation length which represents short range order where phonon can propagate with no damping [41].

2.4 *Glass characterization: optical properties*

Glasses were cut into 1-2 mm thick slices and polished to an optical quality. UV-VIS spectroscopy in transmission was carried out with a Varian Cary 500 spectrometer in order to assess the absorption spectra of the rare earth doped glasses.

Refractive index was measured for all samples at five different wavelengths (533, 825, 1061, 1312 and 1533 nm) by the prism coupling technique (Metricon, model 2010). The resolution of the instrument was of ± 0.0001. Five scans were used for each measurement. Standard deviation in refractive index at different point of the same sample was around ±0.0003.

Bruker Tensor 37 FTIR Spectrophotometer was used to record the infrared (IR) transmittance spectra in the range from 1800 to 7000 cm^{-1}.

The steady-state emission measurements were made with a Ti-sapphire ring laser (0.4 cm^{-1} linewidth) at 793 nm of excitation wavelength. The fluorescence was analyzed with a

0.25 monochromator, and the signal was detected by a PbS detector and finally amplified by a standard lock-in technique. Lifetime measurements were obtained by exciting the samples with a Ti-sapphire laser pumped by a pulsed frequency doubled Nd:YAG laser (9 ns pulse width), and detecting the emission with a Hamamatsu R5509-72 photomultiplier. Data were processed by a Tektronix oscilloscope. All measurements were performed at room temperature.

3. Experimental results

3.1 Prepared samples, DSC and refractive index analyses

Glasses were named using the following scheme: "T" stands for Tm and it is followed by a number indicating the mol % content of Tm^{3+} ions in the prepared glass. Group 'I' in Table 1 refers to FTG host glass in which GeO_2 content was varied whilst the rare earth concentration was kept constant (5 mol% Tm^{3+} ions). Group 'II' corresponded to glasses with constant GeO_2 content (3 mol%) and dopant ion concentration ranging from 1 to 5 mol%. In group 'III' fluoride content was increased, Pb^{2+} concentration was varied together with the way fluorine was incorporated inside the glass (i.e. as PbF_2 instead of PbO) and the dopant concentration was kept constant (3 mol% of Tm^{3+} ions). Group 'IV' glasses were previously investigated [42] and were used as reference samples.

Glass transition temperature values (T_g) are reported in Table 1, together with T_x - T_g values, Tm^{3+} concentration and refractive index at the wavelength of 633 nm.

From Table 1 it is clear that the replacement of ZnF_2 with GeO_2 has a strong influence on thermal stability, crystallization temperature (T_x) shifts significantly to higher temperatures whilst T_g slightly increase. Glass stability also increases with increasing Tm^{3+} content.

All samples show T_x-T_g > 100°C except the first and second 'Group I' glasses, F(0 GeO_2)T5 and F(2.5GeO_2)T5, where a wide crystallization peak with small amplitude is observed. It can thus be concluded that FTG - Tm^{3+} doped glasses have similar stability towards devitrification as typical TZN host composition. In particular, the most stabile TZN – T5 composition has ΔT = 152°C whilst in the case of FTG glass the value slightly increase to 179°C for the F(3GeO_2)T5 sample.

Refractive index values (Tab. 1) first increased with replacing ZnF_2 for low amounts of GeO_2 (group I), but then decreased when GeO_2 was higher than 3 mol%. Refractive index decreased with increasing Tm^{3+} content, similar to Tm^{3+}-doped TZN glasses. FTG glasses, if compared to TZN compositions, show an increase in refractive index of about ~ 0.1 at all wavelengths.

The emission cross section is proportional to the refractive index: $\sigma_{emisssion} \sim (n^2+2)^2/n$ [43] which gives $\sigma_{TZN} = 0.92\sigma_{FTG}$. The first evidence of higher laser emission efficiency of FTG is thus here reported.

3.2 Judd – Ofelt theory results

Judd – Ofelt (J – O) theory is used to calculate transition probabilities between different manifolds, radiative lifetimes, and emission branching ratios. The largest error in J - O calculation is the assumption that all Stark levels of a given multiplet are equally populated ("natural excitation" being assumed) [44]. Fig. 1 shows the absorption cross section for two different hosts, FTG and TZN, doped with the same thulium concentration of 5 mol%. The figure shows that FTG host has higher absorption cross section at both, pump and laser wavelengths.

The line strength of a transition can be obtained from the absorption cross section by using the expression [45]:

$$S_m = \frac{3(2J+1)}{4\pi^2 \alpha \bar{\lambda}} \cdot n\left(\frac{3}{n^2+2}\right)^2 \cdot \int \sigma(\lambda) d\lambda \qquad (4)$$

where $\alpha = 2\pi e^2/(hc) = 7.297\ 10^{-3}$, 'e' is electron charge, 'c' is the speed of the light, 'h' is Planck constant, 'J' is total angular moment of the initial state ($^{2S+1}L_J$), '$\bar{\lambda}$' is the mean wavelength, 'n' is refractive index, and 'σ' is absorption cross section.

J – O parameters 'Ω_λ' can be determined by minimizing the square of the difference between S_m and S_{ED} (electric dipole line strength). The values of J – O parameters of several FTG based glasses are given in Table 2 in comparison with sample T5 which has a TZN glass host.

Physical interpretation of J – O parameters came from experimental observation. For instance it has been shown that Ω_2 parameter increases with the index of refraction while Ω_4 and Ω_6 are quite independent from the index of refraction [44]. Inside the glass matrix, rare earth ions are connected with oxide or fluoride ions through strong covalent bonds which are correlated to J – O intensity parameter Ω_2. It is sensitive to the local structure in RE vicinity and its value increases strongly as the symmetry of environment decreases [46]. In the present work J – O parameters follow the sequence $\Omega_2 > \Omega_4 > \Omega_6$. Parameters Ω_4 and Ω_6 are related to the rigidity of the host medium in which the ions are located. In order to have large emission cross section, high values of Ω_4 and Ω_6 parameters are eligible. Since Ω_2 does not influence branching ratio, the spectroscopic quality factor 'X' ($X = \Omega_4/\Omega_6$) will define fluorescence intensity [45]. Parameters Ω_4 and Ω_6 are insensitive to the local environment, but connected with the RE site degree of covalence. Their values can increase by lowering the covalence of

the chemical bonds between RE ions and ligand anions [44]. The values of J – O parameters vary only slightly with concentration [48]. J – O parameter and reduced matrix product $\Omega_2 \left| \langle \varphi_a \| U^{(2)} \| \varphi_b \rangle \right|^2$ are correlated with Einstein coefficient 'A' and asymmetry in local structure surrounding RE ion while analog product for Ω_4 and Ω_6 corresponds to covalency of RE ion and oxygen ion bonding. Furthermore, 'A' coefficient could give the assumptions about the position of the RE ion inside a glass matrix. Smaller value indicates interstitial and higher substitutional position in the case of Yb^{3+} [49].

Table 2 shows that the covalence given by parameter Ω_2 is decreasing with decreasing amounts of either GeO_2 or Tm^{3+} ions. Section '3.3 Viscosity' will show that this assumption is supported by viscosity values. Furthermore, these values indicate that a higher symmetry corresponds to lower GeO_2 contents. In comparison with TZN host, FTG glasses are more rigid, thus higher viscosities could be expected.

For most of the absorption bands, at least those with $\Delta J \neq 1$, contribution of magnetic dipole is negligible and transition probability (Einstein 'A' coefficient) can be given by:

$$A_{J'J} = \frac{32\pi^3 \alpha c}{3(2J'+1)\bar{\lambda}^3} \cdot n \cdot \left(\frac{n^2+2}{3}\right)^2 \cdot S_{ED} \qquad (5)$$

where S_{ED} is electric dipole(ED) line strength, $\alpha = 2\pi e^2/(hc) = 7.297\ 10^{-3}$, n is refractive index, c is light velocity and J' is total angular momentum of the upper level.

Tm^{3+} absorption bands are all dominated by ED transitions, except for the transition $^3H_6 \rightarrow {}^3H_5$, which also contains magnetic-dipole contributions and can be calculated as previously reported [45].

Results of J – O calculation made for F($3GeO_2$) T5 sample are reported in Table 3 as example.

Table 4 shows radiative lifetime values obtained from J-O analysis for the two different glass hosts.

Differences in radiative lifetime between FTG and TZN thulium doped glasses arise mainly from different refractive index values: host materials with higher refractive index show lower radiative lifetime values, even if this does not correspond to reduced quantum efficiency. J – O theory applied on other FTG samples gave similar results. The radiative lifetime value of $^3F_4$ level is significantly lower than the experimental value of T0.36 sample, whose value, being the re-absorption effect negligible, was taken as the lifetime value of the single ion.

3.3 Viscosity measurements

Viscosity curves of FTG and TZN samples are shown in Figures 2 a, b and c.

Viscosity measurements show that viscosity increased with Tm^{3+} concentration and GeO_2 content (Fig. 2a and 2b) as indicated by J – O parameter 'Ω_2'. Furthermore, the comparison between TZN and FTG host given in Fig. 2c shows that FTG glasses show higher viscosity than TZN glasses for the same dopant concentration. Experimental error in determination of T_g is ±3°C. Fitting parameters of VFTH model are given in Table 5.

Table 5 shows all fitting parameters obtained from the experimental data together with the expected drawing temperatures: the drawing temperature of all glasses is lower than crystallization temperature which guarantees good viscosity for fiber drawing. FTG glasses are expected to be drawn at higher temperatures than corresponding TZN glasses.

3.4 Raman Spectroscopy

Fig. 3 shows characteristic glass peaks: boson peak, Te-O-Te, TeO_4 and TeO_3 bands. Spectra are normalized on the area under TeO_4 and TeO_3 modes and shifted one to the other. The position of TeO_4 peak in the case of FTG glass is shifted towards lower frequency of around 12 cm^{-1}.

Boson peak for both glass systems have unchanged position at 40 cm^{-1}. Using equation (3), phonon correlation length can be estimated to be 22 Å.

For longitudinal ultrasonic velocity the value of similar $75TeO_2 – 25ZnO$ composition, v_l = 3775 m/s is taken [50, 51].

Such value of correlation length is in accordance with the values obtained on binary system $80TeO_2$ - $20Li_2O$ doped with small concentration of Tm^{3+} where cohesive length for spherical shape was equal to 14 Å [41].

3.5 Fluoride influence on reduction of OH content

As previously reported [14], reduced OH atmosphere content during glass fabrication plays an important role in preventing the quenching of the $^3F_4$ emission.

There are several ways to reduce OH content: a) drying of batch chemical powders, b) performing preparation under controlled atmosphere with minimized OH content, c) bubbling the glass melt with carbon tetrachloride CCl_4 or oxygen O_2 [52], d) partial or total substitution of OH^- with F^- (first shown by the introduction of fluoro-oxide glass instead of pure phosphate ones [53]) in order to improve quantum efficiency. The last case can be described by the following reaction: $2[\equiv Te-OH]+ZnF_2 \rightarrow \equiv Te-O-Te\equiv +ZnO+2HF_{(g)}$ [12].

Fig. 4 shows the absorption coefficient calculated as (2.303 Absorbance)/$L_{thickness}$ ($L_{thickness}$ is the sample thickness) of tellurite and fluorotellurite glasses doped with 3 mol% of Tm^{3+}. Spectra are shifted for the presentation purpose.

Glasses show two characteristic peaks in the OH region: strongly hydrogen-bonded OH band (strong OH) at 2250 cm^{-1} and high intensity combination bands of weakly hydrogen-bonded OH band (weak OH) and free OH at around 3000 cm^{-1}. The lowest obtained value of absorption coefficient is 0.24 cm^{-1} (104 dBm^{-1}) for F($3GeO_2$:$14ZnF_2$:5PbO)-T3 sample.

Considering OH region, two features can be observed by comparing FTG and TZN glasses: vanishing of strong OH peak and decrease of weak and free OH combinational band area. OH content can be estimated by equation [54]:

$$N_{OH} = \frac{\alpha \cdot N}{\varepsilon} = 122.65\ 10^{17}\ \alpha \qquad (6)$$

where 'N' is the Avogadro constant, 'ε' is the molar absorptivity of free OH groups in the glass taken as 49.1 10^3 cm^2/mol. It can be assumed that the N_{OH} experimental error is approximately ±0.3 10^{18} cm^{-3}.

An overall strong reduction of OH content was calculated, as reported in Table 6: this is due to the dry atmosphere employed to fabricate the glasses and to the presence of ZnF_2.

However, there are several tasks for which clarification and further examinations are necessary. All the glasses were melted inside the glove box. It should be underlined that powders of fluorotellurite glass components were weighed inside a dry box which was not the case for tellurite glasses (T glasses), so the starting OH content inside the batch powders could give the main contribution to the final OH content of TZN-T3 sample and increase the difference between TZN and FTG glasses. Deviations of OH content in each glass group can be ascribed to possible different powder quality and atmosphere purity inside the glove box. Longer melting process did not show significant difference in the absorption coefficient amplitude. Fluorotellurite glasses with different fluorine content did not show significant

decrease in OH concentration as it would be expected. One of the explanations could be that ZnF_2 content should be strongly increased to have a significant reduction of OH concentration which could contribute to a decrease of glass homogeneity due to evaporation of halide (HF) component. The multiphonon edge did not shift significantly with ZnF_2 content increase.

In this work reduction of OH was performed by batch powder weighing inside the dry box and melting inside the glove box which includes dry-air atmosphere with maximum water content of 0.1 ppmv. The minimum obtained value of absorption coefficient is 0.24 cm^{-1} at the maximum of the weak and free OH band which can be compared with some other processes of OH removal in tellurite glasses. For example, by melt bubbling with CCl_4 and O_2 a value of 1.99 cm^{-1} at 3000 cm^{-1} is obtained [52]. OH content value of about 1.5 10^{20} cm^{-3} can be reached by only O_2 melt bubbling [54]. Significant reduction of OH content is reported for ZnF_2 content higher than 10 mol% in TZN host composition [12]. In the proposed host composition of Nazabal TeO_2:ZnO:ZnF_2 [9] more than 20 mol% of ZnF_2 was needed in order to decrease absorption coefficient lower than 1 cm^{-1}.

3.6 Emission spectra of FTG glasses

The infrared emission in the 1350-2200 nm spectral range was obtained for all samples by exciting at 793 nm. Fig. 5 shows the ratio of the integrated emission intensity of $^3F_4 \rightarrow {}^3H_6$ and $^3H_4 \rightarrow {}^3F_4$ transitions divided by ion concentration whilst abscissa denotes Tm^{3+} concentration in mol%. Strong enhancement of the $^3F_4 \rightarrow {}^3H_6$ emission can be observed in the case of FTG glasses (Group II) in comparison to TZN glass particularly for Tm^{3+} concentrations of 3 and 5 mol%.

Figures 6 a, b, c show the IR emission for FTG and TZN glasses doped with 1, 3, 5 mol% of Tm^{3+} normalized to the $^3F_4 \rightarrow {}^3H_6$ emission.

It is clear that $^3H_4$ emission vanishes quicker as Tm^{3+} increases in FTG glasses than in TZN glasses. Quicker depletion of the $^3H_4$ level means stronger cross-relaxation process ($^3H_4$, $^3H_6 \rightarrow {}^3F_4$, $^3F_4$).

The second effect which could be observed is self-trapping i.e. shifting of $^3F_4$ and $^3H_4$ emission peaks to longer wavelengths which is especially strong in the case of the highest concentration of 5 mol%.

It should be underlined that the fluorescence of all glass groups was measured on the same experimental set up with the same geometry, pump intensity and focus. Measurements of TZN glasses can be considered as including weak self-trapping whilst the reason of stronger FTG glasses self-trapping is still an open question.

3.7 Fluorescence lifetimes of $^3F_4$ level

Decay of the $^3F_4$ level (Group II) can be well approximated by an exponential function for the three different concentrations: 1, 3, 5 mol% Tm^{3+}. Self quenching in the case of dd interaction, for a negligible self-trapping, can be fitted using the formula proposed by Auzel [55]:

$$\tau = \frac{\tau_0}{1 + \frac{9}{2 \cdot \pi}\left(\frac{N}{N_0}\right)^2} \tag{7}$$

where 'τ' is measured lifetime at given concentration 'N', 'τ_0' is lifetime for low concentrations i.e. radiative lifetime, 'N_0' as the critical sensitizer concentrations is linked with critical distance between sensitizer and trap as $R_0 = (3/(4\pi N_0))^{1/3}$.

Fitting the experimentally obtained lifetime values to the above formula (Fig. 7.) gives the characteristic parameters shown in Table 7. The critical distance is longer in TZN glass which indicates faster energy transfer.

Fig. 7 shows clearly that all FTG glasses show enhanced lifetime values if compared to TZN glasses. Thus the presence of both ZnF_2 and GeO_2 are beneficial for the use of these materials as active media in optical fiber lasers.

3.8 Fluorescence lifetimes of $^3H_4$ level

Decay curves of $^3H_4$ level of group 'II' glasses in a semi-logarithmic scale show a non-exponential behavior for all concentrations. Average lifetime values are calculated by using the expression [13]: $\langle\tau\rangle = \frac{1}{I(t=0)} \cdot \int I(t)dt$.

Calculated average lifetime values of $^3H_4$ level for FTG glasses are similar to TZN host glasses (Tab. 8).

Non-exponential decay curves of $^3H_4$ emissions which are attributed to diffusion – limited regime when energy transfer between sensitizers and sensitizer to activator via dipole – dipole interaction occurs can be fitted by the Yokota – Tanimoto (Y-T) equation [55].

$$\phi(t) = \phi(0) \cdot e^{-t/\tau_0} \cdot \exp\left[-\frac{4}{3} \cdot \pi^{3/2} \cdot N \cdot (C \cdot t)^{1/2} \cdot \left(\frac{1+10.87x+15.5x^2}{1+8.743x}\right)^{3/4} \right] \qquad (8)$$

with $x = B \cdot t^{2/3}$ and parameterization $A = \frac{4}{3}\pi^{3/2} \cdot N \cdot C^{1/2}$, B = $DC^{-1/3}$, 'N' is dopant concentration and 'D' is diffusion coefficient. Examples of fitting curves for TZN-T1 and F($3GeO_2$)T1 samples are shown in Fig. 8 a, b.

Parameters obtained from Yokota – Tanimoto fitting are reported in Table 9.

In the case of $^3F_4$ level, energy transfer (ET) parameter C is smaller for FTG glasses than for TZN whilst there is no significant difference in parameter C for $^3H_4$ level regarding TZN and FTG glass host. However, diffusion coefficient slightly decreased in the case of FTG glass. Critical ET distance is about the same for both glass hosts.

4. Discussion

This work compared novel Tm^{3+}-doped glasses based on the host composition $75TeO_2 – xZnF_2 – yGeO_2 – 12PbO – 3Nb_2O_5$ [x(5–15), y(0–5)mol%] with common TZN glass host in terms of thermo-mechanical, optical and spectroscopic properties.

Regarding TZN glasses, their glass transition temperature of about 300 °C and the difference between glass transition and crystallization temperatures higher than 100 °C prove good temperature range and glass stability. Viscosity measurements show a behavior in - between strong and soft glass formers, while the drawing temperature is set in trustful region between glass transition and crystallization temperature. Spectroscopy measurements in highly doped Tm^{3+}:TZN glasses show promising characteristics for optical fiber laser devices as already discussed [42].

In comparison with TZN glass host, FTG host contained a relatively small amount (~ 3 mol %) of GeO_2, which improved their thermal stability. Such improvement is of crucial importance for fiber fabrication process. Viscosity measurements proved possibility of drawing FTG based glass compositions into optical fibers. Refractive index increased for ~0.1 for all FTG types of glasses, which was mostly due to the addition of metal oxides such as PbO and GeO_2. That guarantees the increase in emission cross section of about 8%. Judd-Ofelt theory assumed that the new composition could offer similar spectroscopic properties as the TZN glass. The increase of J – O intensity parameter Ω_2 correlated to covalent bond, is in

accordance with the multiphonon edge shift (Fig. 4) to shorter wavelengths indicating stronger cation – anion bonding [56].

The highest frequency band of Raman spectra showed that the phonon energy did not increase. Fluorine addition did not reduce the overall phonon energy of the glass, but it is still possible to consider that RE ions may dissolve mainly in fluorine rich zones. Red shift of the TeO_4 stretching band frequency in FTG glass host could be indication of a different phonon confinement [57]. Considering phonon energy, a more detailed investigation of local RE ion environment should be carried out in the future. From the boson peak position a phonon diffusion length equal to 22 Å was determined.

Spectroscopy measurements showed a relative increase of the $^3F_4 \rightarrow {}^3H_6$ emission intensity vs. $^3H_4 \rightarrow {}^3F_4$ transition and longer lifetimes for level $^3F_4$ in FTG glasses compared with TZN. It is shown that depletion of $^3H_4$ level occurs faster in the case of FTG host which indicates stronger CR effect. The reason of lifetime increase could be due to the following phenomena: a) lower OH content, b) strong self-trapping, and c) lower phonon energy ion environment. Since strong reduction of OH absorption is observed for FTG glasses, a decrease of OH groups should be one of the reasons of lifetime increase. The fingerprint for self – trapping is a red shift of the emission spectra and a lifetime increase for highly doped samples. The increase of the radiation trapping is expected for the glasses with higher refractive index [58]. On the other hand, thulium is not subject of self-trapping effect as it is for example ytterbium [59]. Furthermore, emission spectra and lifetime measurements were done with the same equipment and conditions i.e. launching the laser beam on a 1-2 mm thick sample edge and collecting the fluorescence light in 90° geometry for TZN-Tm^{3+} and FTG-Tm^{3+} samples. As previously reported [42], no reabsorption effect is observed in the case of TZN glass host. The authors assumed that the presence of slight self-trapping cannot explain the lifetime increase and fluorescence enhancement in comparison with the case of TZN host.

Finally, lower phonon ion environment could be the reason for the increased quantum efficiency of the emission in FTG glasses. However, this is still an open question; FTG glasses need further examinations and results approval. Above all, optical fiber geometry will contribute to self – trapping effect which gives importance to above considerations. There are still many possibilities for fabrication improvement of this novel kind of host composition such as powder drying and glass preparation by using high purity reagents. Furthermore, fluoride content could be increased with certain compensation with GeO_2 which could reduce OH content even more and increase quantum efficiency.

5. Conclusions

In this work, novel active glass compositions $75TeO_2 – xZnF_2 – yGeO_2 – 12PbO – 3Nb_2O_5 – zTm^{3+}$ [x(5–15), y(0–5), z(0-5) mol%] were designed, fabricated and characterized both from a structural and spectroscopic point of view and a full comparison of their properties with the well known TZN glass composition was carried out. The fluorotellurite glasses show lower OH content, higher refractive index, and enhanced quantum efficiency of $^3F_4$ emission. The lower OH content results in enhanced emission intensity from $^3F_4$ level at 1.8 μm and increasing quantum efficiency. On the other hand, the higher refractive index gives an enhanced emission cross section for these fluorotellurite glasses compared with TZN ($\sigma_{TZN} = 0.92\sigma_{FTG}$).

Raman spectroscopy showed a shift of TeO_4 stretching modes to lower frequencies whilst the position of TeO_3 remains the same. Boson peak position defined correlation length as 22 Å. Energy transfer microparameter of $^3F_4$ level ($6.4\ 10^{-54}\ m^6/s$) decreased of about one order of magnitude in comparison with TZN host, whilst in the case of $^3H_4$ level they are about the same, i.e. $\sim 5.44\ 10^{-51}\ m^6/s$.

In particular, for short cavity optical fiber lasers, the 3 mol% Tm^{3+} doped glass sample F($3GeO_2$) T3 showed a trade off in terms of lifetime values and emission intensities with no impairment of thermo – mechanical properties and could be considered as the suitable candidate for fiber drawing.

Acknowledgments

The authors wish to thank the Regione Piemonte Converging Technologies "Hipernano" research project. R. Balda and J. Fernández acknowledge financial support from the Spanish Ministry of Science and Innovation under project MAT2009-14282-C02-02 and from the Basque Country Government (IT-331-07).

References

[1] A. Godard, C. R. Physique 8 (2007) 1100-1128.

[2] C. A. Evans, Z. Ikonic, B. Richards, P. Harrison, A. Jha, J. Lightwave Tech. 27 (19) (2009) 4280-4288.

[3] M. Yamane, Y. Asahara, Glasses for Photonics, Cambridge University Press, ISBN-13: 9780521580533, 2004, 131.

[4] S.Singh, L.G.Van Uitert, W.H.Grodkiewicz, Opt. Commun., 17, (1976), 315.

[5] J.C. Michel, D.Morin and F.Auzel, Rev.Phys.Appliquée, 13, (1978), 859.

[6] J.S. Wang, E.M. Vogel, E. Snitzer, Tellurite glass: a new candidate for fiber devices, Optical Materials 3, (1994), 187-203.

[7] Elizabeth R. Taylor, Li Na Ng, and Neil P. Sessions, Herbert Buerger, Spectroscopy of Tm^{3+} -doped tellurite glasses for 1470 nm fiber amplifier, J. Appl. Phys., vol. 92, no. 1, (2002).

[8] H. Burger, U. Grunke, I. Gugov, Optical tellurite glasses for optical waveguide amplifiers and oscillators, and process for producing them, US Patent 2003/0045421, (2003).

[9] V. Nazabal, S. Todoroki, A. Nukui, T. Matsumoto, S. Suehara, T. Hondo, T. Araki, S. Inoue, C. Rivero, T. Cardinal, J. Non-Cryst. Solids 325, (2003), 85–102.

[10] G. Liao, Q. Chen, J. Xing, H. Gebavi, D. Milanese, M. Fokine, M. Ferrarsi, J. Non-Cryst. Solids 355 (2009) 447–452.

[11] Kobayashi, S., Shibata, N., Shibata, S., and Izawa, T. Rev. Electrical Comm. Lab, 26 (1978), 453-467.

[12] Matthew O'Donnell, Tellurite and fluorotellurite glasses for active and passive fibreoptic waveguides, PhD thesis, University of Nottingham, 2004.

[13] R. Balda, L.M. Lacha, J. Fernandez, J.M. Fernandez-Navarro, Opt. Materials 27 (2005) 1771–1775.

[14] E. R. Taylor, Li Na Ng, Neil P. Sessions, H. Buerger, J. Appl. Phys. 92 (1) (2002) 112-117.

[15] L. M. Fortes, L. F. Santos, M. C. Goncalves, R.M. Almeida, J. Non-Cryst. Solids 324 (1-2) (2003) 150–158.

[16] V.N. Sigaev, I. Gregora, P. Pernice, B. Champagnon, E.N. Smelyanskaya, A. Aronne, P.D. Sarkisov, J. Non-Cryst. Solids 279 (2001) 136-144.

[17] G.Lakshminarayana, J.Qiu, M.G.Brik, I.V.Kityk., J. Phys.: Condens. Matter 20 (33) (2008) 335106.

[18] G.Lakshminarayana, J.Qiu, M.G.Brik, G.A.Kumar, I.V.Kityk, J.Phys.: Condensed Matter 20 (2008) 375101.

[19] A. K. Varshney, Fundamentals of Inorganic Glasses, Academic Press, New York, 1994.

[20] A. Karamazov, R. Di Gioacchino, P. Pisciella, M. Pelino, Glass Technol. 43 (1) (2002) 34 – 8.

[21] Tellurite Glasses Handbook, A. Raouf, H. El Mallawany, CRC Press, ISBN 0849303680, (2001), 199.

[22] M. L. F. Nascimento, C. Aparicio, J. Phy. Chem. Solids, 68 (2007) 104 – 110.

[23] V.M. Fokin, M.L.F. Nascimento, E.D. Zanotto, J. Non - Cryst. Solids 351 (10-11) (2005) 789 – 794.

[24] G.J. Fan, H.Choo, P.K.Liaw, J. non-Cryst. Solids 353 (2007) 102 – 107.

[25] M.L.F. Nascimento, C. Aparicio, Physics B, 398, (2007), 71 – 77.

[26] U. V. Desnica, I. D. Desnica-Frankovic, M. Ivanda, K. Furic, T. E. Haynes, Phys. Review B 55 (24) (1997) 16205-16216.

[27] R. Duverger, M. Bouazaoui, S. Turrell, J. Non - Cryst. Sol. 220 (1997), 169 – 177.

[28] C.C. Yu, Phys. Rev. Lett. 63, (1989), 1160.

[29] V. G. Karpov, M.I. Klinger, F.N. Ignatiev, Zh. Eksp. Teor. Fiz. 84 (1983) 760.

[30] R.Orbach, Science, 231, (1986), 814.

[31] S. Marjanovic, et al. J. Non-Cryst. Sol. 322, (2003), 311-318.

[32] A.G. Kalampounias, S.N. Yannopoulos, G.N. Papatheodorou, J. Non-Crystalline Solids, 352, (2006), 4619–4624.

[33] S.N. Yannopoulos, K.S. Andrikopoulos, G. Ruocco, J. Non-Crystalline Solids. 352, (2006), 4541–4551.

[34] V.K. Tikhomirov, A. Jha , A. Perakis, E. Sarantopoulou, M. Naftaly, V. Krasteva, R. Li, A.B. Seddon, J. Non-Crystalline Solids 256&257 (1999) 89-94.

[35] N. Jaba, A. Mermet, E. Duval, B. Champagnon 351 (2005) 833–837.

[36] F. Pelle, F. Auzel, J. Lumin. 87-89 (2000) 598-600.

[37] H. Lamb, Proc. London Math. Soc. 13, (1882) 189.

[38] E. Duval, A. Boukenter, B. Champagnon, Phys. Rev. Lett. 56, (1986) 7052.

[39] M. Ivanda, K. Furić, S. Musić, M. Ristić, M. Gotić, D. Ristić, A.M. Tonejc, I. Djerdj, M. Montagna, M. Ferrari, A. Chisaera, Y. Jestin, G. C. Righini, W. Kiefer, J. Raman Spectroscopy 38 (2007) 647 -659.

[40] M. Ivanda, K. Babocsi, C. Dem, M. Schmitt, M. Montagna, W. Kiefer, Phys. Rev. B 67 (2003) 235329-235337.

[41] J. C. Sabadel, P. Armand, F. Terki, J. Pelous, D. Cachau-Herreillat, E. Philippot, J. Phy. and Chem. of Solids 61 (2000) 1745-1750.

[42] H. Gebavi, D. Milanese, R. Balda, S. Chaussedent, M. Ferrari, J. Fernandez, M. Ferraris, J. Phy. D. 43 (2010) 135104.

[43] S. Dai, J. Wu, J. Zhang, G. Wang, Z. Jiang, Spectrochimica Acta Part A 62, (2005), 431–437.

[44] F.Auzel, J. Alloys and Compounds 380 (2004) 9–14.

[45] B. M. Walsh, N. P. Barnes, D. J. Reichle, S. Jiang, J. of Non-Crystalline Solids 352, (2006), 5344–5352.

[46] G. Wang, S. Dai, J. Zhang, L. Wen, J. Yang, Z. Jiang, Spectrochimica Acta Part A 64, (2006), 349–354.

[47] G. Lakshminarayana, M. Mao, R. Yang, J.R. Qiu, M.G. Brik, Phy. B. 404 (20) (2009), 3348-3355.

[48] A. Florez, Z. Messaddeq, O.L Malta, M.A. Eagerter, J. Alloys and Compounds, 227, (1995), 135 – 140.

[49] T. Murata, K. Mazeno, K. Morinaga, 3 (2002) 85 – 90.

[50] R. El –Mallawany, Mat. Chem. and Phys. 53 (1998) 93-120.

[51] R. El –Mallawany, J. Appl. Phys. 73 (10) (1993) 4878.

[52] X. Feng, S. Tanabe, T.Hanada, J. non Cryst. Solids 281 (2001) 48 – 54.

[53] F.Auzel, Ann.Telecom. 24 (1969) 199.

[54] S. Dai, C. Yu, G. Zhou, J. Zhang, G. Wang, L. Hu, J. Lumin. 117 (2006) 39–45.

[55] W.E.K. Gibbs, D.J. Booth, V.K. Bogdanov, J. Non-Crystalline Solids 353 (2007) 1–5.

[56] J.E. Shelby, Introduction to Glass Science and Technology, Royal Society of Chemistry, 2nd edition, ISBN: 0854046399, 2005.

[57] M. Yang, D. Huang, P. Hao, F. Zhang, X. Hou, X. Wang, J. Appl. Phys. 75 (l) (1994).

[58] D.S. Sumida, T.Y. Fan, Opt. Lett. 19 (17) (1994) 1343.

[59] F. Auzel, F. Bonfigli, S. Gagliari, G. Baldacchini, J. Lumin. 94–95 (2001) 293–297.

Tables

Table 1. Dopant concentration, thermal characteristics and refractive index values for FTG and TZN host.

Group	*Sample name*	*Tm^{3+} (cm^{20})*	*T_g(°C)*	*T_x-T_g(°C)*	n_{633nm}
I	***F(0GeO_2)T5** 75TeO_2 0GeO_2 10ZnF_2 12PbO 3Nb_2O_5 - 5 mol% Tm^{3+}	10.55	321	46	2.1057
	F(2.5GeO_2)T5 75TeO_2 2.5GeO_2 7.5ZnF_2 12PbO 3Nb_2O_5 -5 mol% Tm^{3+}	10.5	326	99	2.1123
	F(3GeO_2)T5 75TeO_2 3GeO_2 7ZnF_2 12PbO 3Nb_2O_5 -5 mol% Tm^{3+}	10.43	335(323^{DMA})	179	2.1203
	F(5GeO_2)T5 75TeO_2 5GeO_2 5ZnF_2 12PbO 3Nb_2O_5 -5 mol% Tm^{3+}	10.5	333	188	2.1141
II	**F(3GeO_2)T5** 75TeO_2 3GeO_2 7ZnF_2 12PbO 3Nb_2O_5 -5 mol% Tm^{3+}	10.43	335(323^{DMA})	179	2.1203
	F(3GeO_2)T3 75TeO_2 3GeO_2 7ZnF_2 12PbO 3Nb_2O_5 -3 mol% Tm^{3+}	6.37	332(321^{DMA})	170	2.1246
	F(3GeO_2)T1 75TeO_2 3GeO_2 7ZnF_2 12PbO 3Nb_2O_5 -1 mol% Tm^{3+}	2.13	332(317^{DMA})	136	2.1428
III	**F(2.5GeO_2)T3** 75TeO_2 2.5GeO_2 7.5ZnF_2 12PbO 3Nb_2O_5 -3 mol% Tm^{3+}	6.38	320	171	2.1260
	F(5GeO_2:7ZnF_2:10PbF_2)-T3 75TeO_2 5GeO_2 7ZnF_2 10PbF_2 3Nb_2O_5 3 mol% Tm^{3+}	6.61	340	160	2.1193
	F(3GeO_2:14ZnF_2:5PbO)-T3 75TeO_2 3GeO_2 14ZnF_2 5PbO 3Nb_2O_5 -3 mol% Tm^{3+}	6.45	345	172	2.0926
IV	**TZN – T1** 75TeO_2 20ZnO 5Na_2O - 1 mol% Tm^{3+}	2.28	313	124	2.0454
	TZN – T3 75TeO_2 20ZnO 5Na_2O - 3 mol% Tm^{3+}	6.84	322	146	2.0396
	TZN – T5 75TeO_2 20ZnO 5Na_2O - 5 mol% Tm^{3+}	11.3	321	152	2.0306

* FTG without germanium (III) oxide
** T_g and T_x ±3°C

Table 2. Comparison of Tm^{3+} J-O parameters with literature: Ω_λ [10^{-20} cm^2] (λ =2,4,6). TZN – T5 sample is put as the reference and fluorotellurite glasses are listed as the GeO_2 content decrease.

Sample	**Ω_2**	**Ω_4**	**Ω_6**
TZN-T5	4.4	1.97	1.22
F(5GeO_2) T5	4.73	2.14	1.48
F(3GeO_2) T5	4.78	1.86	1.51
F(3GeO_2) T3	4.44	2.19	1.32
F(2.5GeO_2) T3	3.8	1.67	1.21
F(0GeO_2) T5	3.96	1.81	1.37

Table 3. Radiative lifetimes and branching ratios for different energy transitions of the sample F(3GeO_2) T5.

transition	**$\bar{\lambda}$ (nm)**	**$A_{J'J}$ (s^{-1})**	**τ_0 (ms)**	**β**
$^1G_4 \rightarrow {}^3H_6$	470	2914.47	0.18	0.51512
$^1G_4 \rightarrow {}^3F_4$	646	406.26		0.0718
$^1G_4 \rightarrow {}^3H_5$	763	1713.19		0.3028
$^1G_4 \rightarrow {}^3H_4$	1177	506.22		0.08947
$^1G_4 \rightarrow {}^3F_3$	1494	117.73		0.02081
$^3F_3 \rightarrow {}^3H_6$	686	4975.88	0.17	0.84411
$^3F_3 \rightarrow {}^3F_4$	1138	145.5		0.02468
$^3F_3 \rightarrow {}^3H_5$	1558	766.71		0.13006
$^3F_3 \rightarrow {}^3H_4$	5552	6.73		0.00114
$^3H_4 \rightarrow {}^3H_6$	784	3024.55	0.3	0.90839
$^3H_4 \rightarrow {}^3F_4$	1432	246.91		0.07416
$^3H_4 \rightarrow {}^3H_5$	2166	58.11		0.01745
$^3H_5 \rightarrow {}^3H_6$	1225	$514.69+123.8_{MD}$	1.71	0.97839
$^3H_5 \rightarrow {}^3F_4$	4226	14.09		0.0216
$^3F_4 \rightarrow {}^3H_6$	1725	512.38	1.95	1

Table 4. Lifetime values of Tm^{3+} in FTG and TZN glass matrix in comparison.

transition	**τ_0 (ms)** experimental T0.36 sample [14]	**τ_0 (ms)** from J-O T5	**τ_0 (ms)** from J-O $F(3GeO_2)$ T5
$^3F_4 \rightarrow {}^3H_6$	3.09	2.1	1.95
$^3H_5 \rightarrow {}^3H_6$	NA	1.71	1.71
$^3H_4 \rightarrow {}^3F_4$	0.347	0.36	0.3
$^3F_3 \rightarrow {}^3H_6$	NA	0.2	0.17
$^1G_4 \rightarrow {}^3H_6$	NA	0.19	0.18

Table 5. VFTH fitting parameters and drawing temperature (taken A= -5).

Sample	**B**	**T_0**	**R^2 (%)**	**T_g**	**T_x**	**$T_{[Log(\eta) = 4]}$ (°C)**
$F(2.5GeO_2)$ T3	1746 ± 16	201 ± 1	96.5	320	491	395
$F(3GeO_2)$ T1	1660±19	213±2	94.9	332(317^{TMA})	468	397
$F(3GeO_2)$ T3	1778±15	209±1	96.8	332(321^{TMA})	502	406
$F(3GeO_2)$ T5	1843±18	207±2	96.1	335(323^{TMA})	514	412
$F(5GeO_2)$ T5	1752 ± 19	216.2 ± 0.9	98.5	329	621	411
TZN T1	1415±17	217±2	95.1	313	447	374
TZN T5	1627±7	220.2±0.6	99.2	320	469	401

*R^2 is the square of the correlation coefficient

** $T_{[Log(\eta) = 4]}$ ± 5 °C

*** T_g of some glasses is measured with DSC and TMA method

Table 6. Approximate value of OH content.

Group	**N_{OH} 10^{18} (cm^{-3})**
TZN-T3	9.8
$F(3GeO_2{:}14ZnF_2{:}5PbO)$-T3	3
$F(5GeO_2{:}7ZnF_2{:}10PbF_2)$-T3	2.9

Table 7. Parameters obtained by fitting on the proposed curve.

Composition	**τ_0 (ms)**	**N_0 10^{20} (cm^{-3})**	**R^2 (%)**	**R_0 (Å)**	**C (m^6/s)**
TZN	3.29±0.07	4.2±0.1	99.7	8.3	$9.8\ 10^{-53}$
FTG	3.1±0.1	17±2	93.2	5.2	$6.4\ 10^{-54}$

*assumed dd interaction, $R_0^6 = \tau_0 C$.

Table 8. Lifetime values (ms) of $^3H_4$ level.

Tm^{3+} (mol%)	**TZN**	**FTG**
1	0.13	0.128
3	0.017	0.016
5	0.008	0.007

Table 9. Parameters obtained from Yokota –Tanimoto fitting.

$^3H_4$ level	**C 10^{-51} (m^6/s)**	**D 10^{-15} (m^2/s)**	**R^2 (%)**	**A ($s^{-1/2}$)**	**B ($s^{-2/3}$)**	**R_0 (Å)**
TZN-T1	4.93	1.57	99.65	119±1	92±3	10.9
F(3GeO_2)T1	5.44	1.09	99.8	116.8±0.4	62±2	11.1

Figures

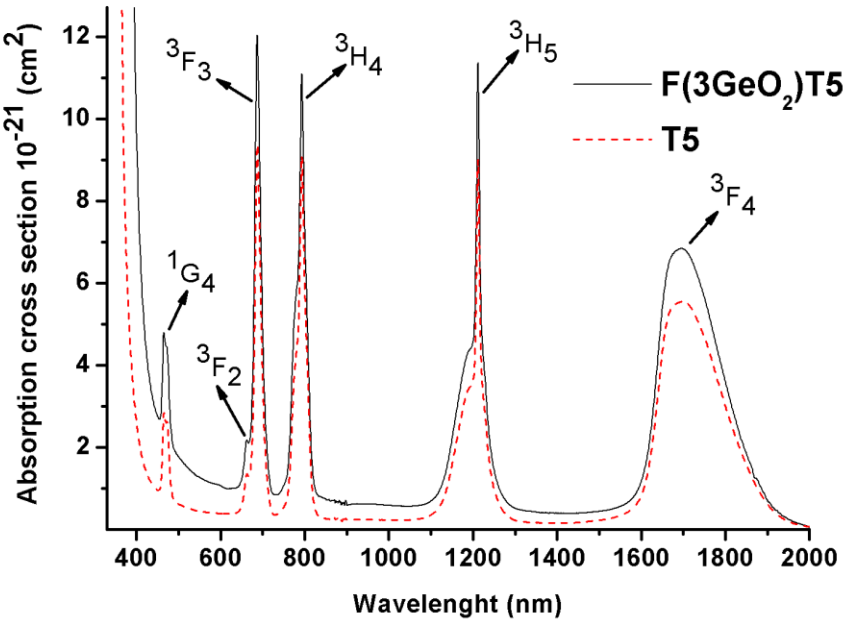

Fig. 1. Absorption cross section of TZN – T5 and F($3GeO_2$) T5 samples.

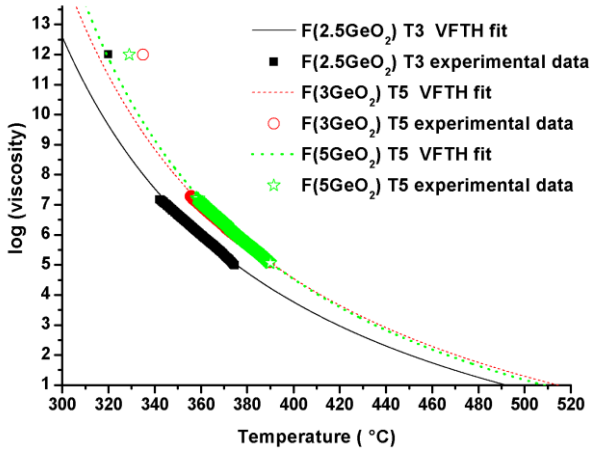

Fig. 2a) Viscosity curves of FTG glasses for different GeO_2 content.

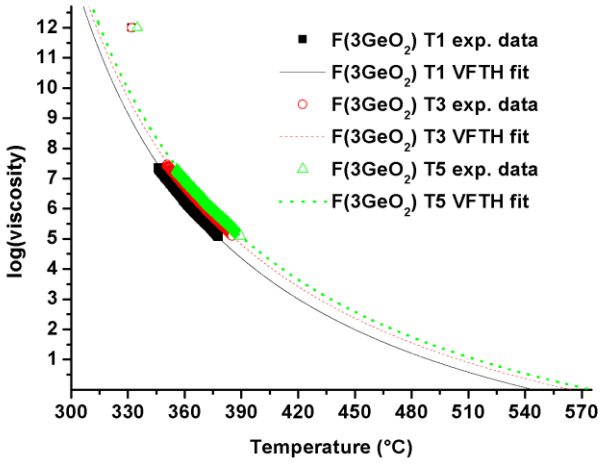

Fig. 2b) Viscosity curves of FTG glasses for different Tm^{3+} concentrations.

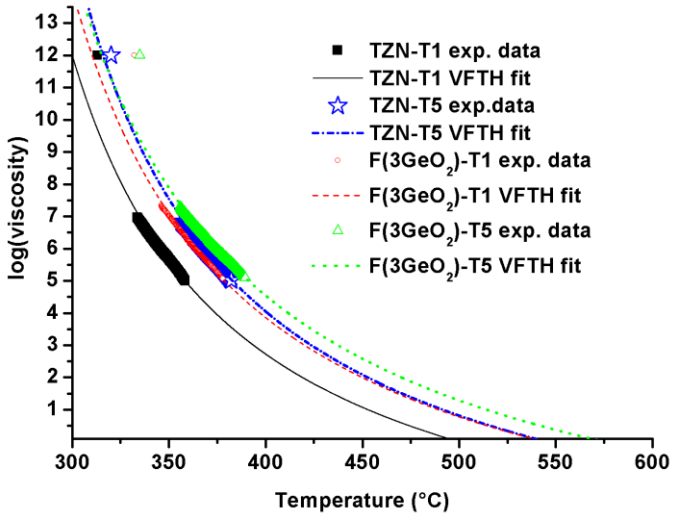

Fig. 2c) Comparison TZN vs. FTG.

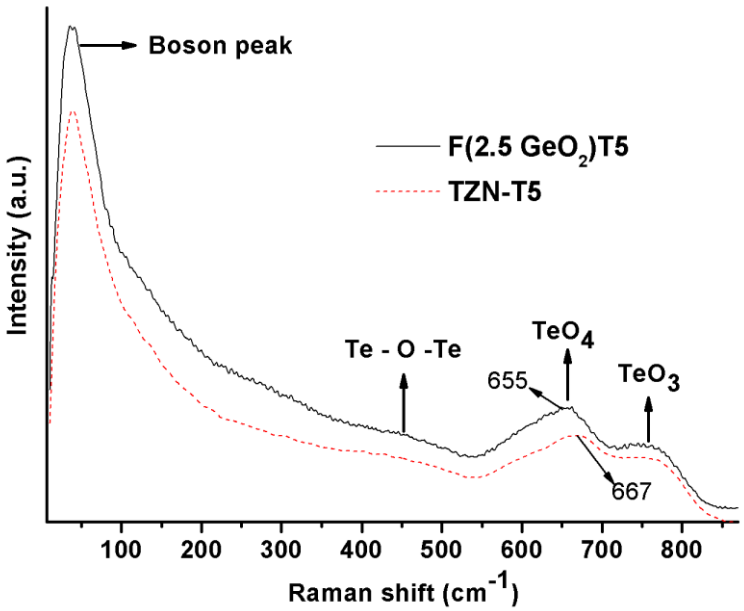

Fig. 3. Raman spectra of TZN and FTG glasses doped with 5 mol% Tm^{3+}.

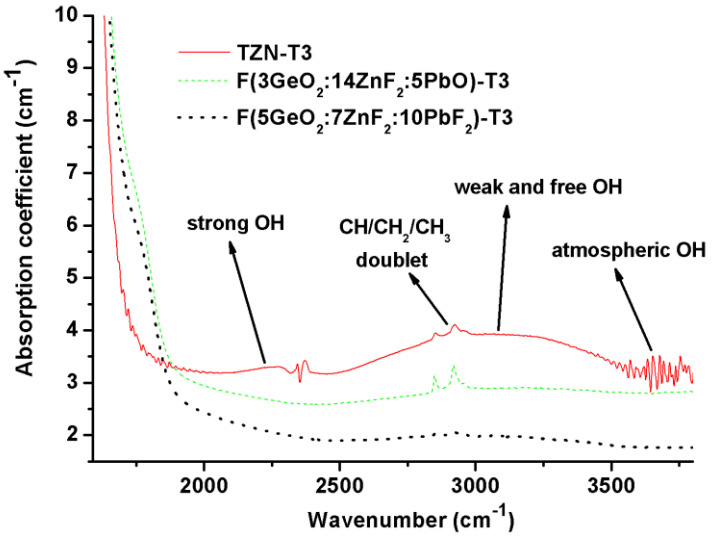

Fig. 4. FTIR spectra of TZN, $F(3GeO_2{:}14ZnF_2{:}5PbO)$ and $F(5GeO_2{:}7ZnF_2{:}10PbF_2)$ doped with 3 mol% of Tm^{3+}.

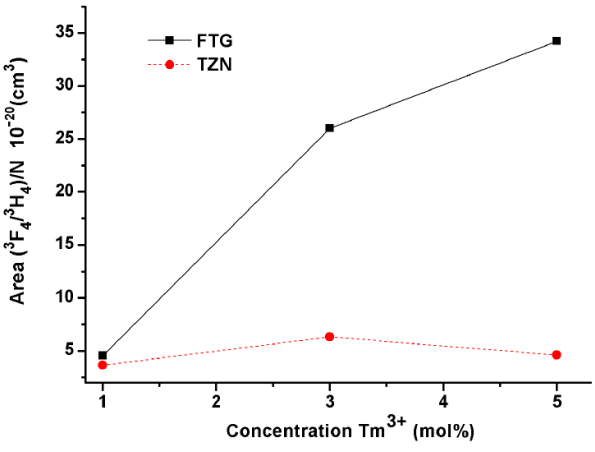

Fig. 5. Area of the peak emission ratio over ion concentration for three different samples of FTG and TZN hosts.

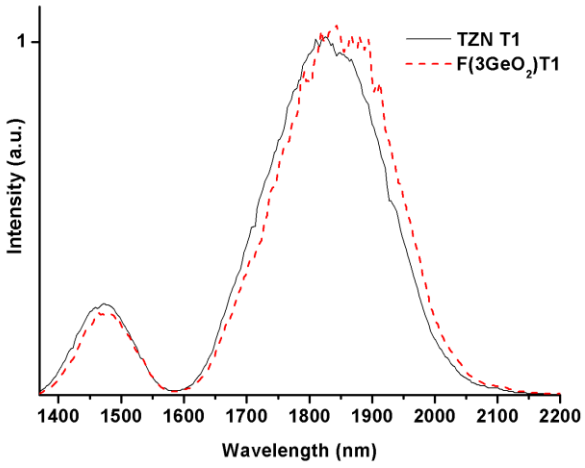

Fig. 6a) Emission spectra of TZN vs. FTG for 1 mol % Tm^{3+}.

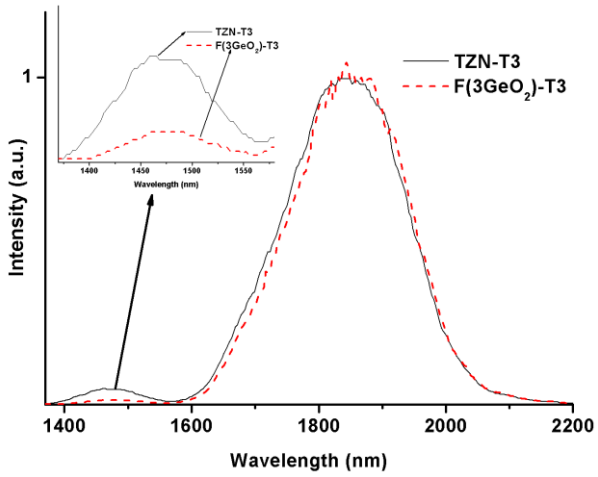

Fig. 6b) Emission spectra of TZN vs. FTG for 3 mol % Tm^{3+}.

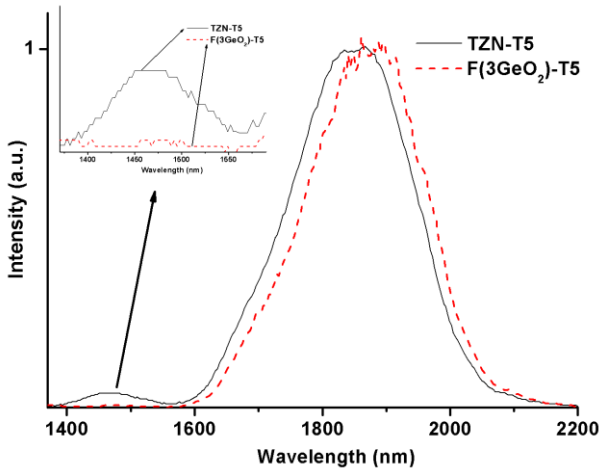

Fig. 6c) Emission spectra of TZN vs. FTG for 5 mol % Tm^{3+}.

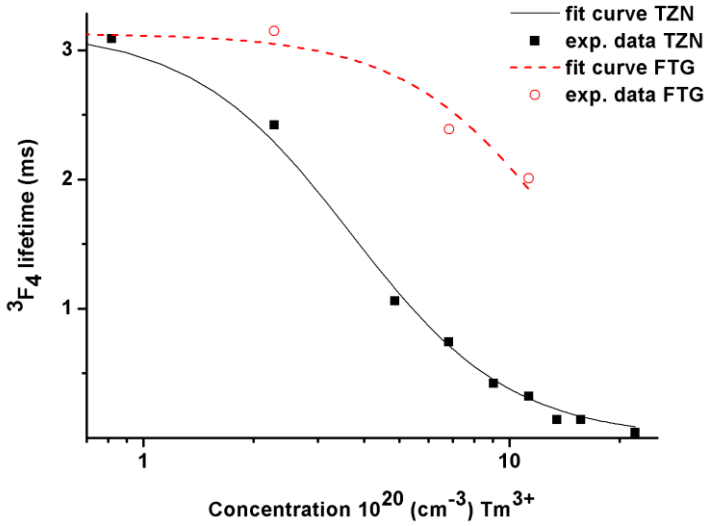

Fig. 7. Lifetime values decay from $^3F_4$ level for various dopant concentrations

* values of TZN group are taken from our previous work [42].

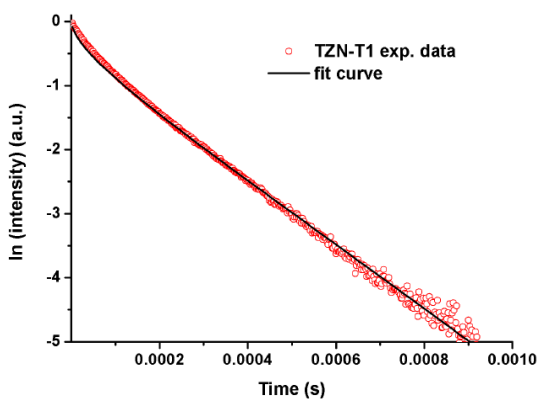

Fig. 8a. Yokota - Tanimoto fit for $^3H_4$ level of the sample TZN-T1.

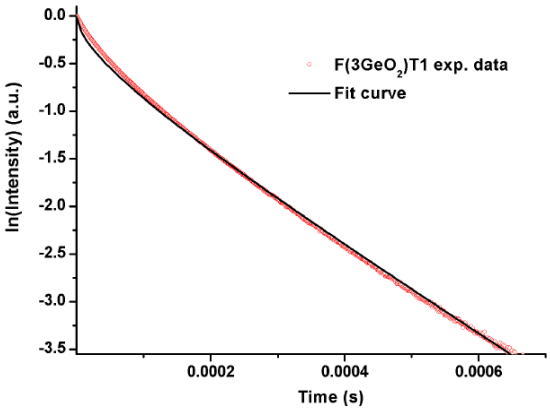

Fig. 8b. Yokota - Tanimoto fit for $^3H_4$ level of the sample $F(3GeO_2)T1$.